https://doi.org/10.22226/2410-3535-2023-2-164-170

Structure of $Ni_{44.4}Mn_{36.2}Sn_{14.9}Cu_{4.5}$ alloy applicable for thermomechanical treatment

R. Yu. Gaifullin[1], K. K. Kirilyuk[2], I. M. Safarov[1], I. I. Musabirov[†,1]

[†]irekmusabirov@mail.ru

[1]Institute for Metals Superplasticity Problems, RAS, Ufa, 450001, Russia
[2]Ufa University of Science and Technology, Ufa, 450076, Russia

Ni-Mn-Sn Heusler alloys exhibit a significant value of magnetocaloric effect. A disadvantage of these alloys is their high brittleness in the as-cast state, but their ductility can be increased by a thermomechanical treatment. The results of a study of thermal treatment for achieving a structure of $Ni_{44.4}Mn_{36.2}Sn_{14.9}Cu_{4.5}$ alloy applicable for further thermomechanical treatment are presented. It is shown that after argon-arc melting and cooling of the ingot in a water-cooled copper crucible, the structure is characterized by two phases that are quite similar in composition and have no clear phase boundaries. After homogenization annealing at 860°C for 24 hours and slow cooling, a two-phase state with regions enriched in Cu atoms is observed. It is possible to preserve the single-phase structure of the high-temperature state by quenching from the annealing temperature. In order to imitate the temperature regime of thermomechanical treatment, the alloy in the single-phase quenched state was subjected to annealing at 700°C for 1 hour and slow cooling. An analysis of the microstructure shows that, as a result, it remains in the same single-phase state. Thus, a mode of heat treatment of the $Ni_{44.4}Mn_{36.2}Sn_{14.9}Cu_{4.5}$ alloy, which makes it possible to achieve the applicable structure for further thermomechanical treatment, was selected.

Keywords: Heusler Ni-Mn-Sn alloys, magnetocaloric effect, structure, energy-dispersive spectroscopy.

1. Introduction

Ni-Mn Heusler alloys based on three or more components attract a wide attention of researchers due to their ferromagnetic shape memory effect (FSME), magnetocaloric effect (MCE), elastocaloric effect (ECE) and others. On single crystal samples, the maximum value of magnetic deformation reaches approximately 12% [1–4], whereas on polycrystalline ones after special preparation it reaches 1–2% [5–8]. The value of magnetocaloric effect is defined through measurements of the step changes of the magnetic entropy ΔS_M (the indirect method) or of the sample temperature (the direct method). In the indirect method, a series of magnetization curves of a sample is measured at different temperatures in the region of the phase transformation. Then, using the Maxwell equation, the change in the magnetic entropy of the sample is calculated. The direct method involves a direct change in the temperature of a sample in the process of rapidly turning on/off the magnetic field. Typically, the value MCE is about 30 J/kg×K [9–12] when measured indirectly and 1 K/T when measured by the direct method [13–16]. Such values of this functional property are quite sufficient for a practical application. But the main obstacle to practical implementation is a very low mechanical strength of Heusler alloys, which leads to a rapid failure of samples under the influence of stresses during thermal cycling in the temperature range of martensitic transformation [17].

The samples obtained by rapid quenching from the melt (RQM tapes) have much higher mechanical properties. Typically, the thickness of the tapes is less than 50 μm. After recrystallization annealing, they exhibit a fine-grained structure and possess high resistance to numerous cycles of martensitic transformation [18,19]. The samples have the same level of MCE values as as-cast alloys [9–11]. However, it is commonly known that obtaining a high-quality tape is quite difficult. The difficulty is obtaining a tape, which is homogeneous in elemental composition and has a uniform thickness for a series of samples. Moreover, the tape thickness of about 50 μm limits its use in magnetocaloric applications. The low mass of a sample will display a low value of heat transfer. Its small thickness will limit the actuator load.

It is known that an enhancement of mechanical properties is most effectively achieved through a thermomechanical treatment (TMT). Heusler alloys can be subjected to severe plastic deformation by torsion (SPDT) [20–23]. Disk-shaped samples 0.3–1 mm thick after recrystallisation annealing have functional values close to the one in as-cast state. However, the annealing allows geting a grain size of 50 μm and less only. A polycrystalline, untextured sample with such a structure will not be able to show high magnetic deformation properties. There are a number of works on extrusion treatment which demonstrate a possibility of achieving a sharp texture [24–26]. This can potentially results in high magnetic deformation characteristics. However, there are no data on an enhancement of mechanical properties in these works.

It is necessary to take into account that a treatment can considerably decrease the values of functional effects due to the size factor of the grain structure, the level of defect

density and the internal stresses. Therefore, the structure of alloy after TMT must provide not only the preservation of increased strength, but also a sufficient value of the functional effect. The authors of the present work have previously shown a significant increase in the cycle and the fatigue strengths of a Ni-Mn-Ga-Si alloy subjected to thermomechanical treatment by forging [27]. An advantage of such a method for Heusler alloys is a resulting microstructure, which consists of large initial grains 100 – 200 μm surrounded by a fine-grained interlayer. The large initial grains will have a functional capacity and demonstrate higher values in comparison with fine-grained samples (RQM, SPDT). The fine-grained structure interlayer will serve as a damper and a drain for stresses caused by phase transformation.

It is known that Ni-Mn-X (X = In, Sn) Heusler alloys, unlike Ni-Mn-Ga Heusler alloys, are usually subjected to quenching from the temperature of homogenization annealing during their smelting, as in the process of slow cooling, phases with different elemental percentage can be formed. Whereas, for the effective TMT it is crucial for the structure of the alloy to be single-phase and equiaxed. Otherwise, a redistribution of the elemental composition of the alloy may take place during treatment of the multiphase state at increased temperatures due to a high diffusion rate. It will finally result in changing of the phase transformation temperatures as the martensitic and magnetic transformations points are very sensitive to the alloy composition [28]. In this case, it is impossible to control the redistribution process.

Thus, it is necessary to conduct a comparative analysis of the microstructure of the alloy obtained by argon-arc melting and subjected to heat treatment in order to achieve a microstructure suitable for further thermomechanical treatment. A four-component Ni-Mn-Sn-Cu ($Ni_{44.4}Mn_{36.2}Sn_{14.9}Cu_{4.5}$) alloy was chosen for the study. According to the literary data, the martensitic transformation point in the alloy with such a composition lies in the region of cryogenic temperatures, which is important for applying MCE for cryogenic uses [29]. The melted alloy was subjected to heat treatment by homogenization annealing and quenching or slow cooling.

2. Material and experimental methods

The $Ni_{44.4}Mn_{36.2}Sn_{14.9}Cu_{4.5}$ alloy to study was prepared from high purity elements by argon-arc melting. The ingot had the mass of about 80 g in order to have a suitable billet volume for TMT. In order to eliminate chemical segregation, a sevenfold remelting of the ingot was carried out. Four samples in the shape of plates 1 mm thick were cut from the ingot. Three plates were sealed into evacuated quartz ampoules and subjected to homogenization annealing (HA) at 860°C for 24 hours, after which two of the samples were quenched in water, and one was cooled at a rate of 5 –10°C/min. One of the quenched samples was sealed again and annealed at 700°C for 1 hour and then cooled at a rate of 5 –10°C/min. Hence, there were four resulting alloy states: state 1 — after argon-arc melting (AAM), state 2 — after homogenization annealing at 860°C for 24 hours and the subsequent quenching (HA860 + Q), state 3 — after HA and the subsequent slow cooling (HA860 + SC), state 4 — annealing of the sample in the state HA860 + Q at 700°C for 1 hour and a subsequent slow cooling (HA860 + Q + AN700 + SC). The last state imitates the temperature regime of thermomechanical treatment — multiaxial isothermal forging at 700°C. The analysis of the microstructure and elemental composition were carried out on a Vega 3-SBH (Tescan) scanning electron microscope equipped with sensors for backscattered electrons and X-Act energy-dispersive analysis (Oxford Instruments). The specimens were prepared by electropolishing in an electrolyte with 90% n-butyl alcohol (C_4H_9OH) and 10% HCl. The melting point and intermediate phase transformations were detected by differential scanning calorimetry. Corresponding measurements were performed on an STA 449 F1 Jupiter instrument (Netzsch). The measurements were taken at heating and cooling rates of 10°C/min.

3. Results and discussion

3.1. Differential scanning calorimetry

Differential scanning calorimetry was carried out in order to define the melting temperature and temperatures of intermediate phase transformations of the alloy in the initial as-cast state. The measurements were taken during the heating of sample to a temperature which was slightly higher than the melting temperature for the given alloys (up to 1100°C) and its cooling to a temperature which was slightly lower than the temperature of the crystallization (900°C).

Figure 1a shows a general view of the curve of the sample heating to 1100°C, which has a large endothermic peak corresponding to the temperature range of the sample melting. In order to identify intermediate phase transformations, an insert with a high heat flux resolution was presented. It is clear that before transition into the melt, two exothermic transformation intervals can be observed: 500 – 650°C and 710 – 800°C. It is known that in Ni-Mn-Ga alloys a transition of the ordered phase with the $L2_1$ lattice type into the partially ordered B2 is observed in a temperature range near 700°C [30, 31]. There are practically no relevant literature data on Ni-Mn-Sn alloys. Some works suggest that this interval lies in a temperature range near 500°C [32]. Thus, it can be assumed that the first interval (500 – 650°C) corresponds to the phase transition $L2_1 \rightarrow B2$. The nature of the transformation in the second temperature range has not been established yet. The melting of the sample occurs in the range of 980 –1080°C with a peak at 1040°C, which corresponds to the melting point. The crystallization process is observed in the range of 1050 – 960°C with two exothermic peaks at 990°C and 1040°C. The presence of the double peak during crystallization is also observed in similar studies of Ni-Mn-Sn alloys, the Sn concentration in which was higher than 13 at.% [33]. The difference between the melting and the crystallization peaks can be explained by a difference in the crystallized structure. As will be shown later (Fig. 2 a), the structure after AAM is characterized by a non-equilibrium state. The degree of non-equilibrium will change depending on the crystallization rate. The peak on DSC curve during the sample heating characterizes a structure, which was rapidly crystallized from the melt while smelting the sample (AAM). Its rate is quite high, since, as it has been mentioned above, the smelting is performed in a water-cooled copper

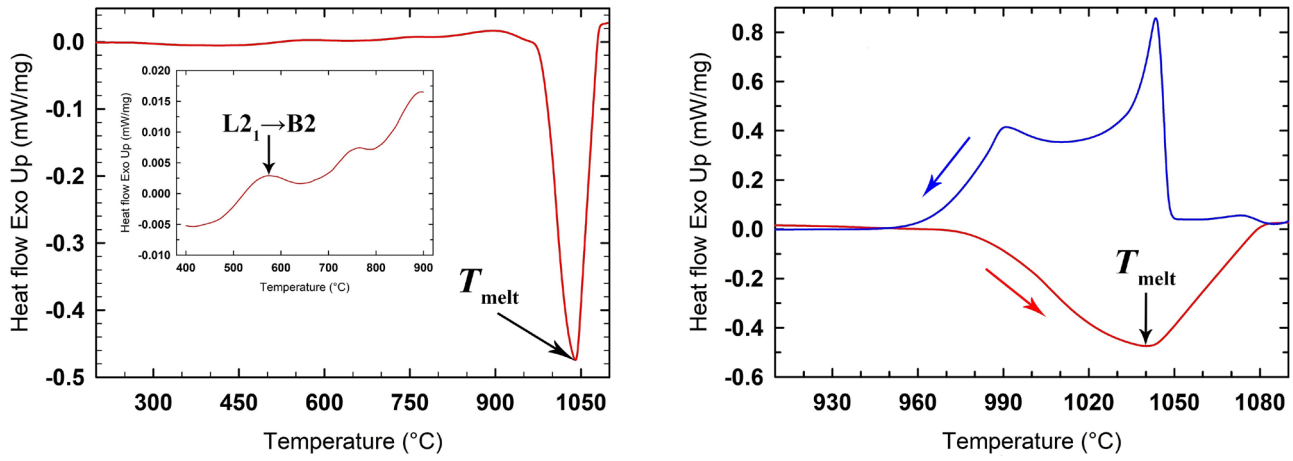

Fig. 1. (Color online) DSC data of the $Ni_{44.4}Mn_{36.2}Sn_{14.9}Cu_{4.5}$ alloy in the state after argon-arc melting (AAM). curve of heating to 1100°C (inset shows the heating section with a higher resolution) (a), heating and cooling curves at the melting point (b).

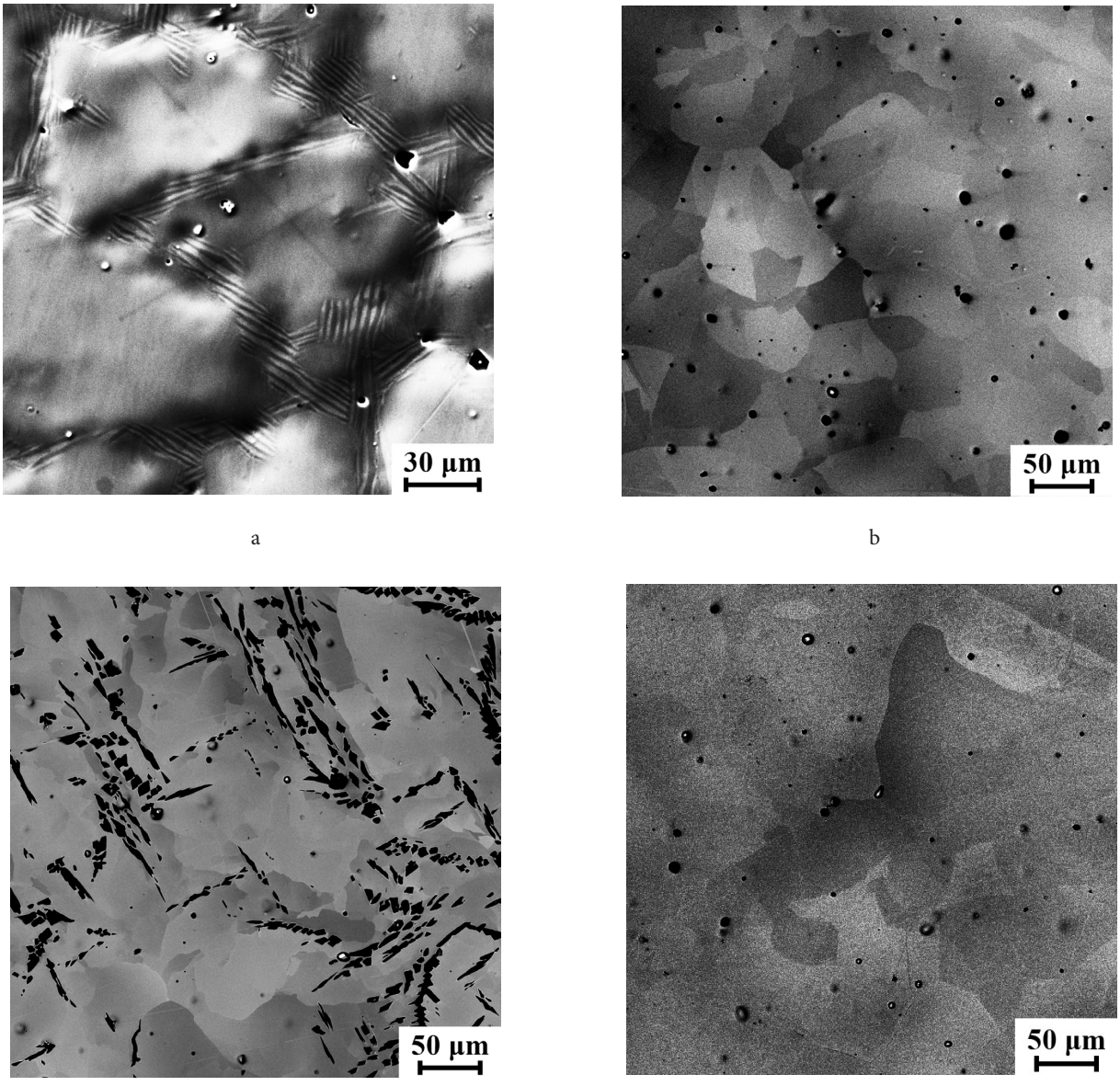

Fig. 2. Microstructure of the $Ni_{44.4}Mn_{36.2}Sn_{14.9}Cu_{4.5}$ alloy in different structural states: AAM (a), HA860 + Q (b), HA860 + SC (c), HA860 + Q + ANN700 + SC (d).

crucible. The peak on DSC curve during the sample cooling characterizes a structure, which is formed at a relevantly slow crystallization rate (10°C/min). It is possible that at such rate of crystallization and cooling a two-phase state is formed. Each of the peaks corresponds to the solidification point of each phase. This statement can be verified through studying the structure of an alloy obtained by crystallization at a cooling rate of 10°C/min. However, attaining such crystallization rate of an ingot in practice is an intractable task.

It is customary to choose homogenization annealing temperature from $0.9T_{melt}$, which in our case corresponds to the temperature of about 910°C. However, in order to exclude a possible melting along the grain boundaries, the temperature of the homogenization annealing in the work was lowered to 860°C.

3.2. The structure of the alloy in various states

The structures of the alloy in four structural states (AAM, HA860 + Q, HA860 + SC and HA860 + Q + ANN700 + SC) are presented in Fig. 2. Figure 2 a represents the structure in the AAM state, i. e., after argon-arc melting. Since the smelting is carried out in a water-cooled copper crucible, the crystallization of the ingot is quite intense and consequently forms a non-equilibrium two-component structure. It consists of uniform-contrast regions characteristic for the austenite phase surrounded by interlayers with a lamellar structure typical for the martensitic phase. The size of the regions equals 100 μm on average. By the X-ray spectral microanalysis it is shown that the phase compositions are $Ni_{45.6}Mn_{32.4}Sn_{19.2}Cu_{2.8}$ and $Ni_{42.1}Mn_{40.4}Sn_{10.1}Cu_{7.4}$, respectively. It should be noted that no clear boundaries between the phases are observed. The formation of a martensitic structure in the second phase indicates that the martensitic transformation point for this composition lies above the room temperature. The lower the melting temperature of an element, the bigger the difference of its concentration in these phases. Nickel (T_{melt}=1453°C) as the most refractory one of the presented elements is distributed uniformly. Manganese (T_{melt}=1243°C) concentration differs by 30%. Concentrations of copper (T_{melt}=1083°C) and the most fusible element tin (T_{melt}=230°C) differ by a factor of two. The presence of pores on a thin section is caused by the method of its preparation. During electropolishing, etching pits or etching of small particles (grains) may occur.

The local enrichment of the elemental composition in the AAM state is demonstrated on the distribution map of chemical elements (Fig. 3). The element maps characterize the differences in the concentrations of elements in the phases. Apparently, the regions represented by martensitic structure began to crystallize first; they are enriched in refractory elements. The regions of the austenite phase crystallized last, which can be seen on the map of the most fusible Sn. As it has been mentioned above, the disadvantage of such a microstructure is its multiphase state. During TMT at high temperatures, a redistribution of the elemental composition of the alloy might take place due to fast diffusion. As a consequence, it may change the temperature of martensitic transformation in the deformed structure. In this case, it is impossible to control the process of changing of the elemental

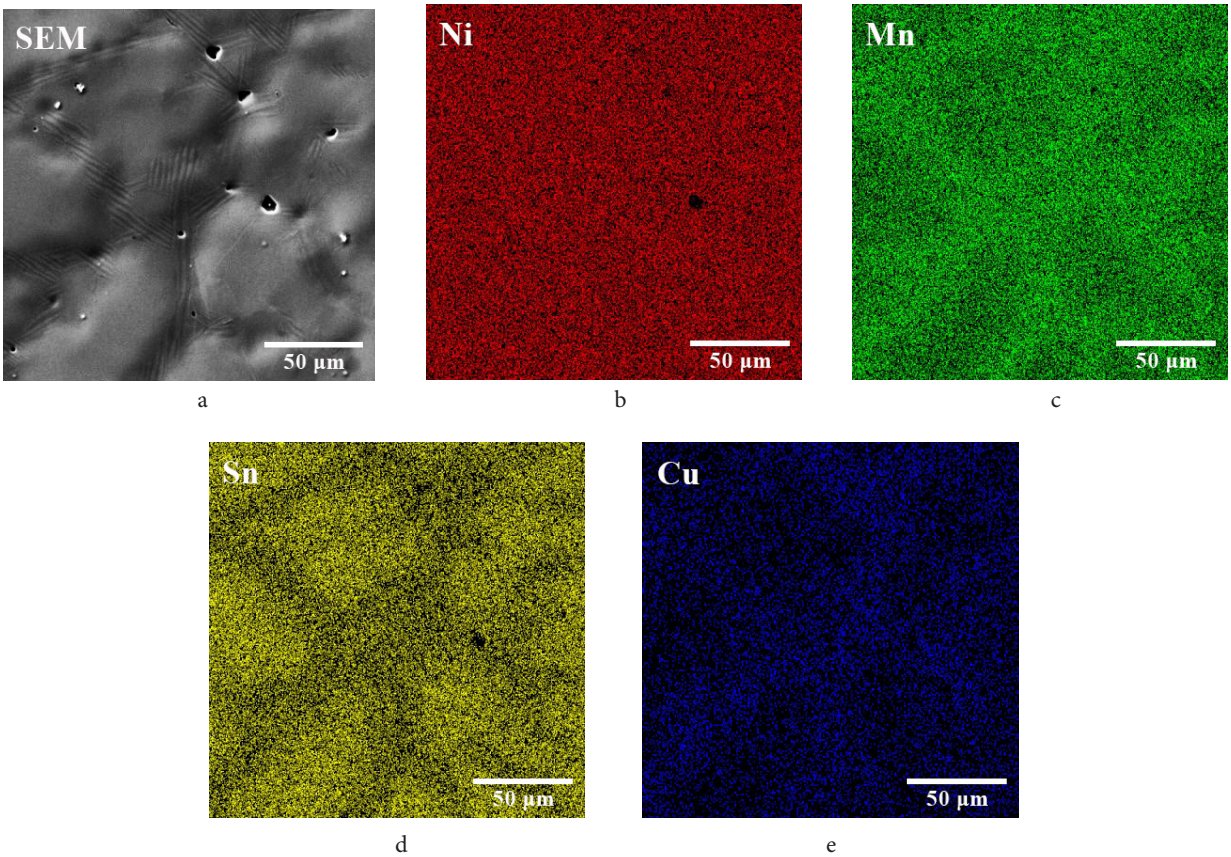

Fig. 3. (Color online) Maps of chemical elements distribution of a section area of the $Ni_{44.4}Mn_{36.2}Sn_{14.9}Cu_{4.5}$ alloy in the state after smelting (AAM).

composition of the phases. Thus, the as-cast structure does not meet the regulatory requirements of being single-phase and having a homogeneous chemical composition.

The microstructure of the alloy after homogenization annealing at 860°C for 24 hours and quenching in water is shown in Fig. 2 b. The homogenization annealing aims to eliminate the inhomogeneity of the elemental composition caused by non-equilibrium crystallization. The structure is represented by a single-phase state. According to the orientational contrast, the grains are 50–150 μm in size. In general, the structure can be characterized as an equiaxed one. A clear, not blurred contrast means that the grain boundaries are high-angle ones. The maps of chemical elements are not presented due to the homogeneous distribution of all the elements, which can also be clearly observed in the orientational contrast mode. It is impossible to detect the presence of inhomogeneity in the distribution of chemical elements on the atomic level by energy-dispersive analysis. The integrated energy-dispersive analysis reveals the composition $Ni_{44.4}Mn_{36.2}Sn_{14.9}Cu_{4.5}$. Thus, the microstructure and the structural state as a result of quenching correspond to the temperature of 860°C. The single-phase state with the practically equiaxed grain structure meets the requirements to the structure for a subsequent thermomechanical treatment.

Most often the quenched state is characterized by a high level of stresses, which can have an impact on further work with the material. For this reason, a microstructure without quenching with slow cooling from the temperature of homogenization annealing was studied. The microstructure after homogenization annealing at 860°C for 24 hours and cooling at a rate of 5–10°C/min is presented in Fig. 2 c. It is clear that the structure is represented by a two-phase state with clear boundaries between the phases. The phase contrast makes it possible to see that one of the phases is lighter in the image than the other. An orientation contrast can be observed against the background of the light phase as well. By the energy-dispersive analysis it is shown that the light phase corresponds to the composition $Ni_{49.1}Mn_{28}Sn_{18.8}Cu_{4.1}$, while the dark phase to the composition $Ni_{56.9}Mn_{29.5}Sn_{3.3}Cu_{10.3}$. The grain size in this phase is approximately 5 μm, which is close to the resolution limit of the energy-dispersive analysis at an accelerating voltage of 20 kV. Therefore, the measured composition of this phase may not exactly represent the actual one.

A map of chemical elements distribution of this section area is presented in Fig. 4. It is clear that dark regions correspond to the phase enriched in Ni-, Mn- and Cu-atoms, while the concentration of Sn in these phases is lowered. As demonstrated above, at the temperature of homogenization annealing the structure is single-phase and the integrated energy-dispersive analysis of the single-phase state reveals the composition $Ni_{44.4}Mn_{36.2}Sn_{14.9}Cu_{4.5}$. During slow cooling of this state a phase with a twofold increase in Cu concentration and a 10% increase in Ni concentration is forming. At the same time, the concentration of Sn is reduced significantly and the concentration of Mn is reduced by 6%. The process of redistribution of elements apparently happens in the temperature intervals of phase transformations (500–650°C and 710–800°C), indicated above in the data of differential scanning calorimetry (Fig. 1). Thus, as well as the state

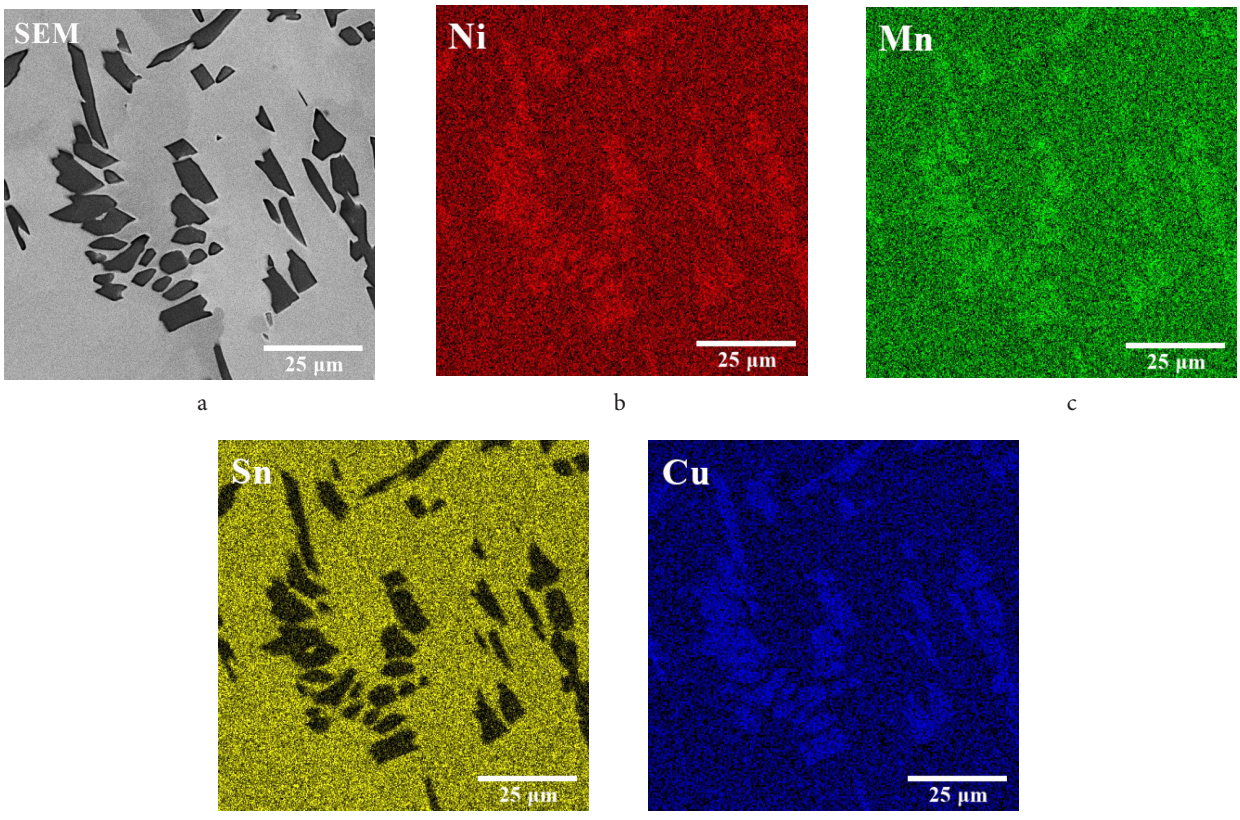

Fig. 4. (Color online) Maps of chemical elements distribution of a section area of the $Ni_{44.4}Mn_{36.2}Sn_{14.9}Cu_{4.5}$ alloy after homogenization annealing at 860°C for 24 hours and slow cooling.

after AAM, the state after the homogenization annealing at 860°C for 24 hours and slow cooling does not meet the applicable requirements of being single-phase and having a homogeneous chemical composition.

Previous works on thermomechanical treatment of Heusler alloys showed that Ni-Mn-Ga alloys plastically deformed at 600 – 700°C [34 – 36]. Therefore, the studied alloy primarily will be subjected to treatment at the same initial temperatures of approximately 700°C. It has been shown above that the structure of HA860 + Q has a single-phase state. For this reason, it is necessary to check the structure after a second heating to 700°C. In order to imitate such temperature regime of the treatment, the alloy after quenching was heated to 700°C for 1 hour and then cooled with a furnace to room temperature. The microstructure of the alloy in this case is identical with the quenched state (Fig. 2 d). It is also characterized with a single-phase state with practically equiaxed grains 50 –150 μm in size. The fact that heating to 700°C for 1 hour does not lead to a destruction of the single-phase state allows one to conclude that the formation of a two-phase state during slow cooling from the HA temperature (Fig. 2 c) must happen in the interval of the second phase transformation (710 – 800°C, Fig. 1).

4. Conclusion

It has beenshown that $Ni_{44.4}Mn_{36.2}Sn_{14.9}Cu_{4.5}$ alloy after argon-arc melting is characterized by a non-equiaxed two-component structure. The presence of a two-phase structure does not meet the requirements of the structure applicable for thermomechanical treatment of the alloy. In order to achieve a single-phase state, it is necessary to perform homogenization annealing with a subsequent quenching into water. As a result, a state with the single-phase structure applicable for TMT, i. e., a state with a homogeneous chemical composition and nearly equiaxed grains 50 –150 μm in size is achieved. The imitation of the temperature regime of thermomechanical treatment is carried out through heating of the sample to 700°C with 1 hour of curing time and cooling with a furnace to room temperature. The single-phase state is not destructed during this treatment. Thus, such structure meets the requirements for thermomechanical treatment with the purpose of enhancing the mechanical properties of the material.

Acknowledgments. The present work was accomplished according to the state assignment of IMSP RAS. The studies were carried out on the facilities of shared services center of the Institute for Metals Superplasticity Problems of Russian Academy of Sciences "Structural and Physical-Mechanical Studies of Materials".

References

1. E. Pagounis, R. Chulist, M. J. Szczerba, M. Laufenberg. Appl. Phys. Let. 105 (5), 052405 (2014). Crossref
2. E. Pagounis, M. J. Szczerba, R. Chulist, M. Laufenberg. Appl. Phys. Let. 107 (15), 152407 (2015). Crossref
3. A. Sozinov, N. Lanska, A. Soroka, W. Zou. Appl. Phys. Let. 102 (2), 021902 (2013). Crossref
4. R. Chulist, E. Pagounis, P. Czaja, N. Schell, H.-G. Brokmeier. Adv. Eng. Mater. 23, 2100131 (2021). Crossref
5. S. Y. Yu, J. J. Wei, S. S. Kang, J. L. Chen, G. H. Wu. J. Alloys and Comp. 586, 328 (2014). Crossref
6. U. Gaitzsch, J. Romberg, M. Potschke, S. Roth, P. Mullner. Scripta Mater. 65, 679 (2011). Crossref
7. U. Gaitzsch, M. Potschke, S. Roth, B. Rellinghaus, L. Schultz. Acta Mater. 57, 365 (2009). Crossref
8. A. A. Mendonca, J. F. Jurado, S. J. Stuard, L. E. L. Silva, G. G. Eslava, L. F. Cohen, L. Ghivelder, A. M. Gomes. J. Alloys Compd. 738, 509 (2018). Crossref
9. S. Dey, R. K. Roy, A. B. Mallick, A. Mitra, A. K. Panda. Materials Today Communications. 17, 140 (2018). Crossref
10. J. Yang, Z. Li, B. Yang, H. Yan, D. Cong, X. Zhao, L. Zuo. Scripta Mater. 224, 115141 (2023). Crossref
11. Y. Zhang, J. Ouyang, X. Wang, Y. Tian, Z. Ren. Mater. Chem. Phys. 290, 126527 (2022). Crossref
12. J. Yang, Z. Li, B. Yang, H. Yan, D. Cong, X. Zhao, L. Zuo. J. Alloys Compd. 892, 162190 (2022). Crossref
13. I. D. Rodionov, Y. S. Koshkidko, J. Cwik, A. Quetz, S. Pandey, A. Aryal, I. S. Dubenko, S. Stadler, N. Ali, I. S. Titov, M. Blinov, M. V. Prudnikova, V. N. Prudnikov, E. Lähderanta, A. B. Granovskii. JETP Lett. 101, 385 (2015). Crossref
14. A. P. Kamantsev, V. V. Koledov, A. V. Mashirov, E. T. Dilmieva, V. G. Shavrov, J. Cwik, A. S. Los, V. I. Nizhankovskii, K. Rogacki, I. S. Tereshina, Y. S. Koshkidko, M. V. Lyange, V. V. Khovaylo, P. Ari-Gur. Journal of Appl. Phys. 117, 163903 (2015). Crossref
15. A. M. Aliev, A. B. Batdalov, L. N. Khanov, A. V. Mashirov, E. T. Dilmieva, V. V. Koledov, V. G. Shavrov. Phys. Solid State. 62, 837 (2020). Crossref
16. Yu. S. Koshkidko, E. T. Dilmieva, A. P. Kamantsev, J. Cwik, K. Rogacki, A. V. Mashirov, V. V. Khovaylo, C. Salazar Mejia, M. A. Zagrebin, V. V. Sokolovskiy, V. D. Buchelnikov, P. Ari-Gur, P. Bhale, V. G. Shavrov, V. V. Koledov. J. Alloys and Comp. 904, 164051 (2022). Crossref
17. W. Everhart, J. Newkirk. Heliyon. 5, e01578 (2019). Crossref
18. V. G. Pushin, E. B. Marchenkova, A. V. Korolev, N. I. Kourov, E. S. Belosludtseva, A. V. Pushin, A. N. Uksusnikov. Physics of the Solid State. 59, 1321 (2017). Crossref
19. E. B. Marchenkova, V. G. Pushin, V. A. Kazantsev, A. V. Korolev, N. I. Kourov, A. V. Pushin. Physics of Metals and Metallography. 119, 936 (2018). Crossref
20. V. Pushin, A. Korolyov, N. Kuranova, E. Marchenkova, Y. Ustyugov. Materials. 15, 2277 (2022). Crossref
21. Y. V. Kaletina, E. D. Greshnova, A. Y. Kaletin. Physics of the Solid State. 61, 2183 (2019). Crossref h
22. R. Chulist, A. Böhm, E. Rybacki, T. Lippmann, C. G. Oertel, W. Skrotzki. Materials Science Forum. 702 – 703, 169 (2011). Crossref
23. R. Chulist, W. Skrotzki, C.-G. Oertel, A. Böhm, T. Lippmann, E. Rybacki. Scripta Materialia. 62, 650 (2010). Crossref
24. R. Chulist, W. Skrotzki, C.-G. Oertel, A. Böhm,

H.-G. Brokmeier, T. Lippmann. International Journal of Materials Research. 103 (5), 575 (2012). Crossref
25. L. Wei, X. Zhang, W. Gan, C. Ding, L. Geng. Scripta Materialia. 168, 28 (2019). Crossref
26. L. Wei, X. Zhang, M. Qian, X. Cui, L. Geng, J. Sun, L. V. Panina, H. Peng. Materials & Design. 112, 339 (2016). Crossref
27. I. I. Musabirov, I. M. Safarov, R. M. Galeyev, D. D. Afonichev, R. Y. Gaifullin, V. S. Kalashnikov, E. T. Dilmieva, V. V. Koledov, S. V. Taskaev, R. R. Mulyukov. Trans. Indian. Inst. Met. 74, 2481 (2021). Crossref
28. T. Bachaga, J. Zhang, M. J. Khitouni, J. Sunol. Int. J. Adv. Manuf. Technol. 103, 2761 (2019). Crossref
29. I. Dincer, Y. Elerman, E. Yüzüak, M. Hölzel, A. Senyshyn, E. Duman, T. Krenke. Acta Crystallographica Section A. 66, s306 (2010). Crossref
30. T. Miyamoto, W. Ito, R. Y. Umetsu, R. Kainuma, T. Kanomata, K. Ishida. Scripta Mater. 62, 151 (2010). Crossref
31. T. Miyamoto, M. Nagasako, R. Kainuma. J. Alloys Compd. 549, 57 (2013). Crossref
32. W. M. Yuhasz, D. L. Schlagel, Q. Xing, K. W. Fennis, R. W. McCallum, T. A. Lograsso. J. Appl. Phys. 105, 07A921 (2009). Crossref
33. D. L. Schlagel, R. W. McCallum, T. A. Lograsso. J. Alloys and Comp. 463, 38 (2008). Crossref
34. I. I. Musabirov, I. M. Safarov, R. M. Galeyev, R. A. Gaisin, V. V. Koledov, R. R. Mulyukov. Phys. Solid. State. 60, 1061 (2018). Crossref
35. I. I. Musabirov, R. M. Galeyev, I. M. Safarov. J. Magn. Magn. Mater. 514, 167160 (2020). Crossref
36. I. I. Musabirov, I. M. Safarov, R. M. Galeyev, D. R. Abdullina, R. Y. Gaifullin, D. D. Afonichev, V. V. Koledov, R. R. Mulyukov. Mater. Phys. Mech. 40, 201 (2018). Crossref